Physics – Uspekhi **60** (2) 149 – 160 (2017)

REVIEWS OF TOPICAL PROBLEMS PACS numbers: 79.20.Ds, 79.20.Eb

Material surface ablation produced by ultrashort laser pulses

A A Ionin, S I Kudryashov, A A Samokhin

DOI: https://doi.org/10.3367/UFNe.2016.09.037974

Contents

Abstract. Various basic mechanisms of material surface ablation produced by ultrashort laser pulses are considered in the order of increasing the supplied laser fluence: low-threshold ultrafast plasma expansion at the electron dynamics stage, spallative ablation, and explosive hydrodynamic supercritical fluid expansion, including the related sequence of basic relaxation processes.

Keywords: ultrashort (femtosecond) laser pulses, surface ablation, ultrafast laser plasma ablation, spallative ablation, shock waves, unloading waves, homogeneous boiling, phase explosion, hydrodynamic supercritical fluid expansion

A A Ionin Lebedev Physical Institute, Russian Academy of Sciences, Leninskii prosp. 53, 119991 Moscow, Russian Federation
E-mail: aion@sci.lebedev.ru
S I Kudryashov Lebedev Physical Institute, Russian Academy of Sciences, Leninskii prosp. 53, 119991 Moscow, Russian Federation;
National Research Nuclear University MEPhI, Kashirskoe shosse 31, 115409 Moscow, Russian Federation;
ITMO University, Kronverkskii prosp. 49, 197101 St. Petersburg, Russian Federation
E-mail: sikudr@sci.lebedev.ru
A A Samokhin Prokhorov General Physics Institute, Russian Academy of Sciences, ul. Vavilova 38, 119991 Moscow, Russian Federation
E-mail: asam@ran.gpi.ru

Received 3 April 2016, revised 27 September 2016
Uspekhi Fizicheskikh Nauk **187** (2) 159 – 172 (2017)
DOI: https://doi.org/10.3367/UFNr.2016.09.037974
Translated by M N Sapozhnikov; edited by A M Semikhatov

1. Introduction

1.1 Specific features of ablation by ultrashort laser pulses

We review work on the removal (ablation) of materials produced by ultrashort [femtosecond, subpicosecond, and short picosecond (< 3 ps)] laser pulses, which has been extensively investigated over the last 30 years for the development of precision and highly efficient processing of the surface of various materials: metals, semiconductors, and dielectrics (including polymers). This work is based on the use of both well-known and new mechanisms and important advantages of the short duration and high peak power (intensity) of ultrashort laser pulses. The work discussed in this review was preceded by quite prolonged investigations using picosecond ($\sim 15-30$ ps), subnanosecond, and nanosecond lasers [1–5], which are currently experiencing a new stage in their development with the advent of high-power and efficient diode-pumped fiber lasers. These lasers deserve a separate detailed consideration, which is beyond the scope of this review.

Nevertheless, about 30 years ago, it was the advent of ultrashort pulse lasers that opened a new page in the history of laser ablation investigations. It is remarkable that this is related not to the different principles of generating ultrashort and short laser pulses [6] but to the characteristic time scales of electron–phonon relaxation in electronically excited materials (Fig. 1) falling exactly in the range $\sim 1-10$ ps [7, 8] between these laser pulse durations. As a result, it was found that unlike the predominantly thermal action of picosecond pulses [9–12], irradiation by ultrashort laser pulses allows initiating a number of fundamentally new, mainly electronic, physical effects in the electron subsystem of materials. They include the separation of electron and lattice temperatures [13, 14], bremmstrahlung of nonthermal

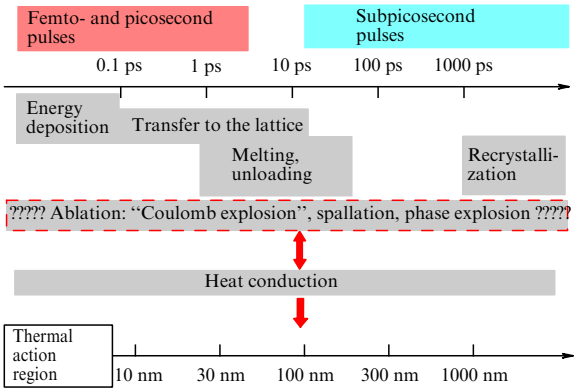

Figure 1. Temporal diagram of the physical processes representing femtosecond laser ablation and the corresponding spatial resolution for different assumed ablation mechanisms determined by the size of the 'thermal action' region by the onset of matter ablation. Numerous question marks indicate the uncertainty of the time scales of basic mechanisms of femtosecond laser ablation. For comparison, the time scales of action of ultrashort and short laser pulses are shown.

electrons [15], changes in the instant optical parameters of materials due to the electronic renormalization of the band spectrum (for example, forbidden gap narrowing [16–18]) and occupation of states [19, 20], intense photo and (or) thermally stimulated and hybrid electron emission [21– 23], and nonlinear emission of fast ions [24]. We note that some of these effects, such as electron temperature separation and electron emission, were studied even before the advent of ultrashort laser pulses, but mainly theoretically [25].

1.2 Brief history of studies

Studies of ablation by ultrashort laser pulses (hereafter referred to as femtosecond laser ablation) were initiated in the early 1980s with the advent of high-power mode-locked lasers in some leading laboratories [26] (see also review [9]) where ultrashort pulses were generated. These lasers were used to study many fundamental phenomena taking place in the interaction of laser radiation with materials in the ablation regime (at fluences from 0.1 to 10 J cm^{-2} and intensities from 1 to 10 TW cm^{-2}), assuming an ultrashort energy deposition with a high peak power [27]. Because of the minimal self-action effect of ultrashort laser pulses (mainly only on the electron dynamics and related optics of photoexcited materials, but without interaction with an ablation plume), the principal feature of femtosecond laser ablation is a complicated multi-scale but completely predetermined spatiotemporal sequence of elementary relaxation processes (see Section 1.3 and Fig. 1).

Correspondingly, different component processes of femtosecond laser ablation were studied until the late 1990s in several areas: by relatively simple time-resolved optical methods (reflectometry, transmission) with femtosecond time resolution [28–31] and standard methods of optical profilometry [32] and mass spectrometry [33–35]. It was found that the high peak power of low-energy ultrashort laser pulses inherent in them due to their short duration allows performing instant electromagnetic adjustment of optical characteristics of materials during excitation times of the electron subsystem at the ultrashort laser pulse scale, for example, to transform a dielectric into a semiconductor [16–18, 36]. In addition, basic ablation regimes were established: hydrodynamic supercritical fluid expansion (phase explosion) [28, 29], vaporization [37, 38], and spallation of a part of the melt layer [31], although the last was also long treated as the hydrodynamic expansion of a two-phase vapor–droplet system [39]. Based on the initial data obtained at this stage, attempts were made to explain femtosecond laser ablation theoretically using the vaporization and hydrodynamic approaches [38, 40, 41] and molecular dynamics [42] with rather simplified but sometimes not even qualitatively correct simulation of basic processes.

Later, with the advent of the first commercial ultrashort pulse lasers and their rather wide applications in the late 1990s, the interaction of intense laser pulses with the surface of condensed materials in the ablation regime was studied more extensively nearly all over the world. This resulted in a great increase in the number of papers devoted to both fundamental studies (generation of high-energy states of matter [43, 44] and high-power shock waves [45–47], emission of charged particles [24]) and practical applications for precise nano- and microscale processing of various materials, including dielectrics [48–50]. As a result, several new physical phenomena have been discovered in the last decade in the ablation regime of the interaction of ultrashort laser pulses with condensed matter: ultrafast plasma emission [51–53], stabilization of the density of photoexcited carriers with a considerable renormalization of the band spectrum [18, 54], and undersurface boiling and foam formation [55–60]. As a whole, a quite large number of experimental facts refining the adopted concepts were obtained. Theoretical studies were also developed further, resulting in a significant qualitative (and sometimes even quantitative) refinement of the picture of femtosecond laser ablation, including spallative ablation [55, 58] and explosive expansion of the supercritical fluid [61, 62]. Important phenomena in the electron dynamics were also predicted, for example, a strong influence of the electron density of states on the dynamics of electron–phonon interaction and the electron heat conduction of materials with complex electronic spectra [63–65].

1.3 Unsolved problems

The complete picture of femtosecond laser ablation does not exist so far because of its complicated interdisciplinary and multiscale nature. This field covers the physics and optics of solid (electron–hole) plasma or hot electron gas, the physics of electron–phonon and phonon–phonon effects in solids, the physics of heat transfer, phase, and chemical transformations, and the hydrodynamics of ablated material flows. However, the construction of a complete picture of femtosecond laser ablation is very important because it gives the characteristic time scales of developing basic ablation processes determining the size of the so-called heat-affected zone at the initial instant of material removal, thereby specifying the spatial resolution for these ablation mechanisms and the specific efficiency of material removal (see Fig. 1).

At the same time, the key potential to elucidate the fundamental mechanisms of femtosecond laser ablation exists because short laser pulses initiate a long multiscale chain in various electronic and lattice processes with predetermined dynamics, which is no longer further affected directly by laser radiation. This concerns first of all the absorption of ultrashort laser pulses, which occurs without the influence of an ablation laser plume, and also various nonlinear thermal laser self-action processes with optical

feedback (unlike the action of short laser pulses). Briefly, such intense absorption of ultrashort laser pulses at the laser pulse scale proceeds via intra- and interband (often nonlinear) optical electronic excitation and related processes governing the absorption and reflection of the surface of a photoexcited material due to the instant change to its optical characteristics (up to absorption saturation), predominantly via the occupation of bands: the heating, thermalization, and emission of electrons (and heat conduction to a lesser extent). At this stage, Auger recombination, the inertialess screening of the ion core by carriers, and the electron renormalization of the band spectrum also occur in semiconductors and dielectrics. The volume energy density deposited at this stage specifies the sequence of relaxation processes, including ablation. Then the deposited energy is gradually transferred at the picosecond time scale for the electron subsystem of the photoexcited surface layer of the material to its ion (lattice) subsystem (electron–phonon relaxation). This is a well-known process, but it was only recently found that it depends on the preceding electron dynamics, in particular, on the instant electron temperature or the electron-induced surface disordering. The surface layer melting then occurs via the mechanisms of homogenous or heterogeneous melting and formation of a hot, inertially compressed subcritical or supercritical fluid experiencing acoustic unloading. During the latter process, finally, depending on the volume density of the initially deposited laser energy, the picosecond irreversible hydrodynamic expansion of the supercritical fluid occurs or the unloaded layer of the melt breaks with the spallation of its nanometer-thick film. Ablation is terminated by melt solidification at the nanosecond or subnanosecond time scale due to the heat transport inside the material and to a lesser extent due to vaporization cooling. Thus, based on the predetermined dynamics of the basic states of femtosecond laser ablation schematically considered above, it is possible to study its stages in detail, from the absorption of ultrashort laser pulses to the ablation of the material and the eventual thermal relaxation. Advances in this field and unsolved problems are considered in the next sections.

2. Electron dynamics and ultrafast 'cold' ablation

2.1 Brief history and basic research methods

It was assumed at the first stage of studies that in contrast to the case of irradiation by short laser pulses, the absorption of ultrashort laser pulses by the surface of a condensed phase in the ablation regime occurs without interaction with the screening (absorbing and scattering) gaseous erosion electron–ion plasma produced after a laser pulse and dynamically changing the absorbing power of the target. At the same time, systematic experimental studies have shown that the absorbing power of condensed targets themselves already changes significantly during ultrashort pump laser pulses due to the electron-gas heating in metals and the generation and heating of electron–ion plasma in semiconductors and dielectrics [14, 16–20, 26, 28, 29, 59]. In the ablation regime produced by ultrashort laser pulses, the dependences of the reflection coefficient on the pump fluence and time for various materials (metals, semimetals, and semiconductors) exhibited a plateau. For semiconductors, based on the measurements of surface second harmonic generation [66–68] and time-resolved X-ray diffraction [69], this effect was attributed to the ultrafast disordering ('nonthermal melting') of a surface layer for a plasma density $\sim 10^{22}$ cm^{-3}. Other possible factors affecting the electron and lattice dynamics, such as the renormalization of the band spectrum (plasma-induced narrowing of the forbidden gap up to its collapse [16]), the balance of ionization and recombination, and electron and plasma-emission effects, were studied only theoretically, not in their totality [18, 54] but taking important factors into account separately [70–72]. These factors include the ion potential screening by plasma, the renormalization of the band gap, the occupation of states, the dispersion of the mass of carriers, and the relaxation of carriers.

2.2 Optical diagnostics of the electron dynamics

In addition, the possibility of a low-threshold plasma yield from the surface of condensed targets irradiated by ultrashort laser pulses in the ablation regime in time-resolved optical [28] and mass-spectrometric studies [34, 73, 74] has been pointed out. However, no direct evidence of such a plasma yield existed and the ion yield estimate seemed to be not sufficiently correct because the same part of the target was irradiated by many ultrashort laser pulses to achieve efficient ablation (possibly of a thermal nature at the pico-nanosecond time scale [33, 34]). This is commonly related to the formation of diffraction periodic surface structures and the local amplification of electromagnetic fields in such structures [9]. Sometimes, along with ion emission, the electron emission was measured [24], assuming an inertialess plasma yield without the establishment of equilibrium between the electron subsystem and the lattice. However, no additional correlation studies of emission have been performed to confirm the inertialess behavior at the ultrashort pump laser pulse scale. Moreover, it is impossible to find such a correlation even in mass-spectrometric experiments with double pumping by variable-delay short laser pulses [34, 73], unlike processes with virtual excitation of carriers such as harmonic generation in nonlinear crystals, because the absorbing power itself evolves after pumping by the first ultrashort laser pulse [14, 16–20, 26, 28, 29, 59]. Nevertheless, some experiments on multipulse femtosecond laser ablation of the surface of dielectrics have been interpreted in terms of the 'Coulomb explosion' [75], which was confirmed by numerical calculations of charging of the surface of dielectrics sufficient for the emission of ions [70], unlike the weak charging of the surface of semiconductors and metals [76, 77].

2.3 Emission of charged particles and surface charging

At the same time, because a material with the electron subsystem strongly excited by an ultrashort laser pulse can in principle become a low-temperature gas plasma, the ultrafast emission of plasma can be expected even for metals for which the absence of surface charging due to the electron emission during ablation by ultrashort laser pulses was predicted theoretically [70]. We note that in contrast to metals, strong surface charging was detected for semiconductors [76, 77]. The intense electron emission and surface charging can be stimulated by the high electron temperature T produced during an ultrashort laser pulse on the surface of metals, semiconductors, and semimetals. This, together with the high-intensity pulsed electromagnetic field, facilitates thermally photo-induced and mixed (Fowler–du Bridge model) processes of N-photon emission of electrons over many possible channels J_N for the laser radiation intensity I and frequency ω and the generalized multiphoton ionization

cross section σ_N [22, 23, 70]:

$$J = \sum_0^\infty J_N\,, \qquad J_N = \sigma_N I^N\,,$$

$$\sigma_N = a_N A_N \left[\frac{e}{\hbar\omega}\,(1-R)\right]^N T^2 F(X_N)\,,$$

$$X_N = \frac{N\hbar\omega - \Phi}{k_\mathrm{B} T}\,, \tag{1}$$

where e is the electron charge, Φ is the work function, k_B is the Boltzmann constant, $\hbar$ is the Planck constant, R is the reflection coefficient, and other parameters and the function $F(X)$ are defined in the Fowler–du Bridge theory [23]. The nonthermal ion yield was detected previously by mass spectrometric and collector methods [24, 34, 73, 74, 78, 79] and interpreted in terms of the Coulomb explosion of a charged surface.

In recent years, experiments have also been performed on the low-vacuum collector detection of electron and ion emission in the ablation regime with single ultrashort laser pulses (to avoid the formation of relief and emission related to the resonance or nonresonance plasmon amplification from the relief structure) [51–53, 80, 81]. The electric circuit developed for the extraction of charges in air directly from the ablation region (ablation target, a grounded electrode) produced high extracting fields up to 3 kV cm^{-1} (in particular, 300 V per mm gap). As a result, the electron emission was studied for the positive (but not negative) collector potential considerably exceeding typical saturation thresholds for emission signals in a vacuum due to a volume charge (of the order of a few mJ cm^{-2}), up to the plasma formation threshold from 0.1 to 1 J cm^{-2}, and the plasma yield itself was also investigated in a broad range of F with signals identical for both polarities of the collector [52]. The threshold yield of charged plasma particles detected by the collector electrode correlated with the yield of positive ions and neutral particles in the optical emission spectroscopy of the ablation plume. Special experiments were also performed for measuring contributions from a filamentation plasma, and direct photoemission from the collector surface and voltampere characteristics were measured for different interelectrode gaps, different incident energy densities, and different numbers of ultrashort laser pulses incident on a point. Because of the development of filamentation in air in front of a target when the energy density threshold for the plasma yield was considerably exceeded (usually, $> 2-3$ J cm^{-2}) and the peak power of ultrashort laser pulses caused the saturation of plasma emission, studies by this collector method were also performed in a vacuum in the absence of filamentations. These investigations were performed in a broad range of laser pulse energies (0.10–20 J cm^{-2}) with weaker extracting fields and confirmed the nonlinear plasma yield with respect to the fluence.

It was found in [51–53, 80, 81] that for a variety of materials such as aluminum, copper, titanium, silicon, and graphite, electron emission below the plasma formation threshold occurs, in fact, linearly. Above this threshold, the emission of charges of both signs is nonlinear, with the exponent varying from 2 (titanium) to 4 (silicon), with the intermediate value 3 (aluminum, graphite, copper). For a copper target, the quantitative agreement was achieved with the data of vacuum probe measurements [24] for the threshold and the power dependence of the electron and ion yield. At the same time, it is very important that for the second, above-threshold laser regime, a correlation was found between the electron–ion plasma yield and the saturation of the reflection coefficient of an ultrashort laser pump pulse or a weak probe ultrashort laser pulse as a function of the pump pulse energy density for all materials: aluminum, copper, titanium, silicon, and graphite (Fig. 2). We note that the existence of such a plasma has been hypothetically assumed for the last two decades based on measurements of the emission of charged particles [24] or the subpicosecond optical reflectometry of graphite [28]. This universality of the effect was attributed to the achievement of high electronic temperatures for such conducting or weakly conducting materials, resulting in strongly thermally (photo) stimulated electron emission and surface charging, which was removed during plasma emission (Fig. 3). In this case, despite the minimal ablation of the surface layer (about a few nanometers [51]), such a low threshold of the electron–ion plasma leads to high plasma-ablation energy losses from the sample surface, freezing the heating of the electronic subsystem at the level of a few electron volts. (See studies of the energy balance for aluminum and silicon at different time scales in Sections 2.4 and 4.2.) Therefore, this effect should be taken into account in the energy balance and dynamics of the electron temperature of materials.

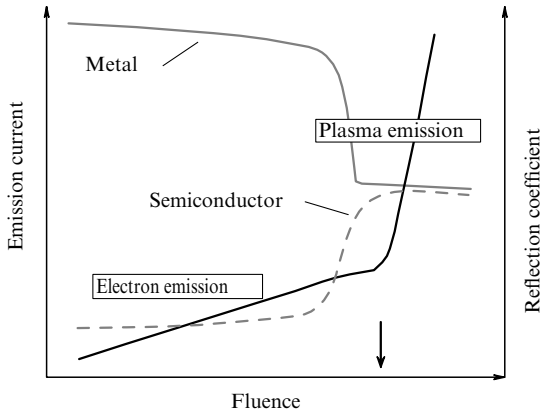

Figure 2. Schematic representation of the correlation of dependences of the emission current in electron and plasma emission regimes (dark curve) and the reflection coefficient for a probe or pump pulse (grey solid curve: metals, dashed curve: semiconductors) on the fluence [51–53].

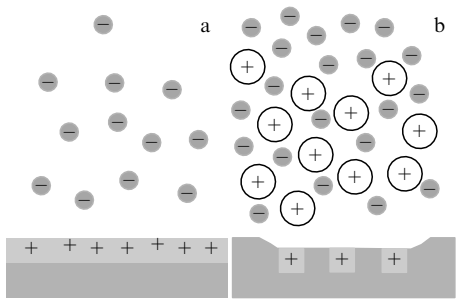

Figure 3. Schematic representation of (a) surface charging processes during intense electron emission from the surface of materials irradiated by an ultrashort laser pulse and (b) the removal of charging via the flying apart of a double electron–ion layer.

We note that various phenomenological models of the ultrafast ablation of surface of materials based on the concept of electron pressure in electronically excited materials have been proposed in the last decade [44, 82–87]. In these papers, kinetic [82] or thermodynamic [83–87] approaches were used to respectively consider the redistribution of the initial homogeneous electron density in the skin layer of a material with the electron temperature gradient and the possibility of initiating material expansion caused by the huge electron pressure of free carriers (ignoring instant transfer effects) [84],

$$\rho\left(\frac{\mathrm{d}V}{\mathrm{d}t}\right) = -\frac{\partial\,(P_\mathrm{e} + P_\mathrm{i} + q)}{\partial z}\,, \tag{2}$$

where ρ in the material density, V is the expansion velocity, $P_{\mathrm{e,i}}$ is the pressure in the electron and ion subsystems, and q is the artificial viscosity in the total system of hydrodynamic equations resembling generalized equations of the two-temperature model for the electron and ion subsystems [25]. Because the second approach is based on plasma theory, electron–phonon coupling problems, in particular, the quantum kinetics of the emission of acoustic phonons producing the hydrodynamic pressure of matter and its ablation expansion, were not actually considered. Such an approach is partially justified only for high degrees of surface charging produced by high-intensity ultrashort laser pulses and (or) high electron temperatures when the material adhesion considerably decreases due to a decrease in the electron density [88], and the material can continuously transform into a plasma-like state.

2.4 Excitation and relaxation of the electron subsystem

The relaxation of the excited but thermalized electron subsystem of materials is traditionally described in the two-temperature model for the electron (T_e) and ion (T_i) subsystems with the respective heat capacities C_e and C_i related to the electron–phonon coupling constant G_e and the electron–phonon relaxation time $\tau_\mathrm{ep} \approx C_\mathrm{i}/G_\mathrm{e}$ [25]:

$$C_\mathrm{e}\frac{\partial T_\mathrm{e}}{\partial t} = \frac{\partial}{\partial z}\left(\kappa_\mathrm{e}\frac{\partial T_\mathrm{e}}{\partial z}\right) - G_\mathrm{e}(T_\mathrm{e} - T_\mathrm{i}) + Q^*\,,$$

$$C_\mathrm{i}\frac{\partial T_\mathrm{i}}{\partial t} = \frac{\partial}{\partial z}\left(\kappa_\mathrm{i}\frac{\partial T_\mathrm{i}}{\partial z}\right) + G_\mathrm{e}(T_\mathrm{e} - T_\mathrm{i})\,, \tag{3}$$

where the effective source can be defined, for example, by taking the above-mentioned thermo/photoelectron-emission and laser-plasma ablation effects into account [51–53, 80, 81] in the form [89]

$$Q^* = (1 - R)\,\alpha I - \frac{J_\mathrm{e}(T_\mathrm{e})}{l_\mathrm{esc}}\exp\left[-\frac{z}{l_\mathrm{esc}}\right], \tag{4}$$

where κ_e and κ_i are the electron and lattice heat conduction coefficients, R and α are the reflection and absorption coefficients of a material for the intensity I, and J_e is the electron flux with the characteristic depth l_esc.

This model of energy transfer from the electron subsystem to the lattice was developed almost half a century ago to study the bombardment of materials by fast ions. The model was considerably corrected in the last decade to obtain the accurate dependences of the coefficients of electron heat capacity, heat conduction, and electron–phonon coupling on the electron temperature T_e, with nonmonotonic energy distributions of the electronic density of states for metals with a complex electronic structure (for example, transition metals [63–65]) taken into account. However, these dependences have been systematically verified experimentally so far only for a few materials by measuring the thresholds of spallative ablation and phase explosion as functions of the duration of picosecond and subpicosecond pulses [89]. It was assumed that the minimum laser ablation threshold is reached for a pulse duration close to the characteristic electron–phonon relaxation time, because the intensity of electronic dissipative processes (emission and high-temperature electron heat conduction) decreases with decreasing the electron temperature as the pulse duration increases to this value (with a simultaneous decrease in thresholds). On the other hand, when this value is exceeded, thresholds increase as the contribution to losses of the electronic heat conduction at lattice temperatures increases. In some cases, for example, for semiconductors, the formulation of the two-temperature model was refined as regards the transport of a dense electron–hole plasma (ambipolar diffusion) and thermalization of the absorbed energy. However, because the reference experimental values of key parameters such as the electron–phonon coupling coefficient were unknown, this coefficient was possibly estimated with a great error [90, 91].

At the same time, most theoretical work disregards the electron and plasma emission in the two-temperature model [9–11, 14, 15, 24, 35, 43, 44, 63, 64] unless the aim of the study is the thermoelectron emission itself [21, 25, 51]. The complete consideration of all linear and nonlinear photoemission, thermoemission, and mixed photo/thermoemission channels, for example, in the Fowler–du Bridge model generalized to take multiphoton processes into account [92], can provide a rather detailed description of electron emission [22, 23, 70]. This description could probably be used to explain the linear electron yield and nonlinear electron/ion yield observed in experiments on increasing the energy density of an ultrashort laser pulse [21, 24 , 34, 51–53, 73, 74, 80, 81]. However, such a complete description of electron emission in the two-temperature model has not been used until how.

Finally, an important but previously neglected effect of the electron dynamics in electron–phonon relaxation in the ablation regime is the ultrafast disordering of the surface of materials accompanying their charging and plasma emission [53], which can drastically accelerate energy transfer from the electron subsystem to the lattice. This can explain short electron–phonon relaxation times (~ 1 ps) measured for various materials (silicon, copper, aluminum, and silver) [93, 94], which are many times shorter than their predicted theoretical values (see, e.g., [64]). These short relaxation times determine not only the smaller size of the thermal action region due to the fast relaxation of strong gradients of the electron temperature but also the higher temperature of the ion subsystem and, correspondingly, the higher rate of thermal phase transformations during ablation.

2.5 Below-threshold nanoscale modification of a surface relief

Despite the minimal ablation of a surface layer in the ultrafast plasma emission regime produced by an ultrashort laser pulse at a depth of a few nanometers [51], it is in this regime that the unusual nanoscale multipulse periodic modification of a surface relief with a period 2–15 times smaller than the pump pulse wavelength was discovered [95–98]. It is interesting that such a laser nanostructuring of material surfaces is

possible only below the corresponding thermally induced spallative ablation threshold for these materials. This is explained by the following reasons: (i) above the threshold, thermal ablation occurs over all the above-threshold region and removes the surface relief; and (ii) weak but ultrafast ablation via plasma emission makes it possible to fix, in the form of the surface relief, the submicroscale or even nanoscale interference distribution of electromagnetic fields of incident ultrashort laser pulses and surface electromagnetic waves with a minimal thermal spread of interference maxima even for metals with high heat conduction (for example, aluminum [60, 99]). As a result, for ultrashort laser pulses with fluences considerably below the spallative ablation threshold, the local spatially periodic ablation of the surface of various dielectrics and metals (in particular, aluminum), is achieved only in interference maxima with the generation of nanoscale spatially periodic structures [60, 95–99]. Their periods correspond to the doubled wavenumber of a short-wavelength surface plasmon resonance due to excitation of a standing wave by counter-propagating surface plasmons [98]. The nanoscale surface relief obtained for materials with the characteristic size of its elements around the size of a vapor bubble ($\sim 10-100$ nm) is of interest for controlling their wetting and liquid boiling in thermophysical setups.

Thus, despite rather numerous but highly specialized experimental and theoretical studies of the electron dynamics and related ultrafast femtosecond laser ablation (reflection and emission of electrons and (or) ions, surface charging, and subablation surface nanostructuring), a complete picture of the electron dynamics of materials in the ablation regime taking the roles of all the above-mentioned effects into account is still lacking.

3. Spallative ablation

3.1 Brief history and basic research methods

Spallation usually means the 'cold' break of a solid target caused by a frontal strike, explosion, or high-intensity laser pulse [1, 2, 100–103] generating a high-power direct shock wave rapidly propagating in the target and reflected from its rear side in the form of a backward (nonshock) rarefaction wave. The last is added with the direct rarefaction wave formed during the unloading of the shock region on the frontal side, and the material breaks in the region where the rarefaction waves add, such that the 'ingot' exits from the rear side of the target (Fig. 4a).

A similar 'two-wave' picture was first used to explain the nanosecond lift-off of a melted film of a material during the spallative ablation of the surface of semiconductors and metals produced by ultrashort laser pulses, demonstrating Newton's interference rings known in classical optics, but in a dynamic version [31, 40] (Fig. 5). Although these rings were first explained using a hypothesis about the scattering of a vapor–droplet mixture as the effective medium with a high

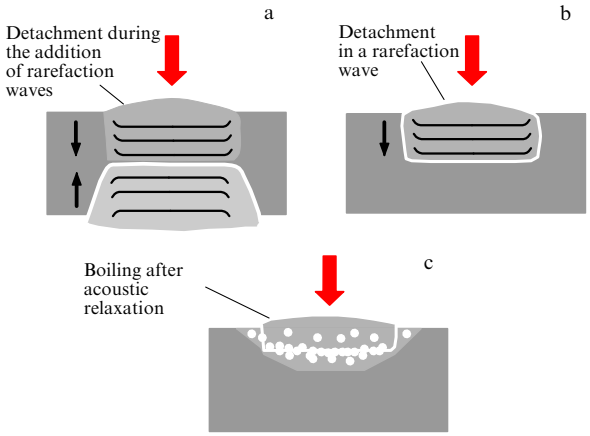

Figure 4. Illustration of basic assumed mechanisms of the detachment of a melt film during femtosecond laser ablation: (a) two-wave mechanism with a rarefaction wave (reflected compression wave) and a direct rarefaction wave; (b) thermomechanical mechanism with a direct rarefaction wave; (c) mechanism related to the expansion of an undersurface vapor cavity.

refractive index [39], the interference model has always been considered after that [31, 40, 59]. This model accounts for the reflection of a probe ultrashort laser pulse normally incident on a target from the surface of a partially transparent film flying away from a microscopic ($\sim 30-100$ μm) region of the visible metal melt, the reflection of its replica transmitted through this film from the melt surface under the film, and their interference on the film surface observed with an optical microscope in the time-resolved reflection regime. (The setup of an optical microscope operating in the reflection regime with stationary illumination replaced by a low-intensity probe ultrashort laser pulse is presented in [31].) As a result, the traditional 'two-wave' model of spallative ablation was used to explain this frontal spallation, assuming that in the inertially heated surface layer inside the target, the phase appearing during the ultrafast heating of a high-power compression wave is reversed [40]. The direct surface unloading wave and the reflected rarefaction wave then interact during acoustic unloading times, which is followed by the spallation of the melt film.

3.2 Relation between the effects of stress unloading and boiling during spallative ablation: extreme cases. Segregation of chemical elements

Subsequent simulations of the removal and lift-off of a melt film during spallative ablation produced by ultrashort laser pulses in the framework of molecular dynamics were performed under the influence of the first papers [40, 41] and involved the thermomechanical removal of the film, but only in the direct rarefaction traveling wave [55, 61, 105–109] (Fig. 4b). This approach is based on observations of the

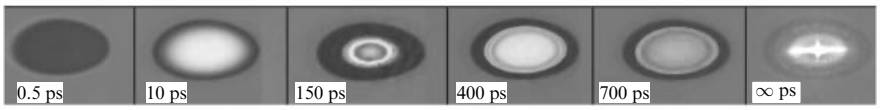

Figure 5. Dynamics of Newton's interference rings on the surface of silicon ablated by an ultrashort laser pulse illuminated by a normally incident ultrashort probe laser pulse (adapted from [104]).

laser-induced undersurface boiling and detachment of a liquid film in a rarefaction wave in transparent 'soft' volume media like gels [110] and weakly absorbing liquids [111–113]. The threshold detachment was still assumed to be related to overcoming the tensile strength during acoustic unloading of the melt, although some authors [55, 57] also considered the undersurface boiling of liquids, which was confirmed by independent studies [56, 57, 59, 60]. Subsequent, more detailed molecular dynamics calculations revealed distinct nanoscale foam formation that not only accompanies the film detachment and inertial formation of nanocusps [55, 57] but also, due to the finite foam elasticity, can cause the return of the film to the surface with a negative velocity [56]. Based on various theoretical estimates of contributions of the rarefaction wave and volume boiling, it was assumed in some papers that the melt film is detached in the phase of completed acoustic relaxation [57, 59, 60] (Fig. 4c) when the melt is in a quasi-equilibrium thermally expanded state (at normal pressure) and has a certain time window for undersurface boiling, which is determined by its cooling due to heat transport.

We note that a qualitatively similar problem was solved previously in the technology of laser cleaning of critical surfaces in microelectronics, where absorbing surfaces were heated by nanosecond laser pulses through a layer of a low-boiling transparent liquid, usually water or isopropyl alcohol [57, 112–115]. It was found that the threshold near-critical boiling of liquid occurs for subnanosecond times [114, 115]; the lift-off velocity of the liquid film above the boiling threshold is independent of the laser energy density [116] and is inversely proportional to the film thickness [113]. In addition, acoustic studies were performed and the time dynamics of pressure in a boiling near-wall layer of a liquid film were analyzed during the growth and percolation of bubbles [117]. The characteristic time scales of percolation were estimated in [117–119] and it was assumed in [120] that pressure in the nanofoam drastically increases during its entry into a microscopic vapor cavity of the layer because of a sharp decrease in the role of surface tension stabilizing vapor bubbles, counterbalancing the vapor pressure [120].

Similarly, the formation of a lateral vapor cavity in the material boiling plane during spallative ablation produced by an ultrashort laser pulse can be indicated by plane spallative craters observed in this case [59, 60, 89]. The depth of such spallative craters observed during femtosecond laser ablation is independent of the ultrashort laser pulse energy density in the entire interval ($\approx 50\%$ of the palliative ablation threshold [59, 89]) between the spallative ablation and phase explosion thresholds, whereas above the phase explosion threshold, the crater depth rapidly increases with increasing the pump fluence (Fig. 6). (To date, it has not been established whether contributions from the surface phase explosion and undersurface spallative ablation are summed in the latter case, and if they are not, then why the depth of the final crater exceeds the spallative ablation depth.) Similarly, the undersurface boiling is directly manifested in the segregation of chemical elements in the near-surface layer, in particular, the depletion of the surface with a more volatile element during ablation nanostructuring of the surface of GaAs chemical compounds by ultrashort laser pulses [121]. Finally, this mechanism is also confirmed by mass-spectrometric studies of femtosecond laser ablation of Si and GaAs [33]: for both these materials, beginning from the spallative ablation threshold (approximately twice as large as the thermal boiling threshold), the

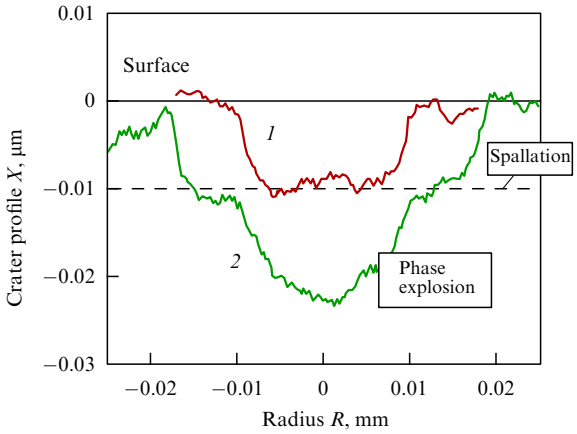

Figure 6. Craters produced on the surface of iron during single-pulse femtosecond laser ablation with the peak fluence (1) above the spallative ablation threshold and (2) above the phase explosion threshold. In the second case, a double structure of the crater with the external plane spallative crater and internal nonplane explosive crater is observed (figure adapted from [89]).

melt surface temperature exceeds 3×10^3 K, and the yield of atoms and positive atomic ions has the character of developed near-critical vaporization. The yield increases with increasing the laser pulse fluence quite rapidly and nonlinearly (nearly quadratically), but at the same time it increases slowly compared to the exponential below-threshold yield [33].

A dynamic analysis of the interference effect (Newton's rings) during spallative femtosecond laser ablation gave qualitatively similar results (see Fig. 5). It was taken into account that depending on the distance of the film flying away from the surface, Newton's rings in the form of illumination maxima and minima in reflection were observed both on the film surface at different instants of time and with time at a chosen point of the film with a fixed local fluence of the ultrashort laser pulse. The velocity of the film flying away as a function of the ultrashort laser pulse fluence was determined from the slope of the time dependence of interference maxima and minima, assuming the weakly refracting vapor phase in the gap under the film ($n \approx 1$ for a probe ultrashort laser pulse) [33, 59, 122]. The minimum velocity (possibly with a subsequent change of sign [123, 124]) was measured near the edge of the spallative crater and the maximum velocity (up to a few kilometers per second) [31, 59, 122, 123] near the phase explosion threshold, which forms within picoseconds in the form of a microheterogeneous strongly scattering vapor–droplet mixture [33, 59, 122, 123]. Moreover, recently the same dependences, with their extrapolation to the zero lift-off distance, were used to study the delay time of the film detachment from the surface as a function of laser radiation fluence [59, 122, 123]. This time rapidly decreased in the subnanosecond time range upon increasing the ultrashort laser pulse fluence, always greatly exceeding the characteristic unloading time of the melt layer. The obtained hyperbolic dependence of the delay time of the film detachment on the ultrashort laser pulse fluence above the ablation threshold (with time delays from a few dozen to a few hundred picoseconds) suggested the explosive nature of boiling preceding the film detachment [59, 121–123].

The evaporative nature of the unloaded film detachment during ablation of the iron surface by ultrashort laser pulses was confirmed by the dependences of the ablation depth for the spallative and phase explosion mechanisms on the fluence

of picosecond and subpicosecond laser pulses [89]. It was reported in [89] that the depth of a spallative ablation crater was in fact independent of the ultrashort laser pulse duration in a broad range from 0.3 to 11 ps. In this case, the electron–phonon relaxation time for a given pump level was 1–2 ps, which tentatively suggests that spallative ablation proceeds considerably later after the pulse end (even for picosecond pulses). Moreover, as the laser pulse duration increased, the slope of the dependence of the ablation depth caused by the phase explosion on the radiation fluence rapidly decreased monotonically to the complete suppression of this mechanism for the pulse duration exceeding 6 ps. The suppression of the phase explosion at long durations of ultrashort laser pulses was attributed in [89] to continuous evaporative cooling of the material surface, which drastically increases, as shown by the yield of atoms and atomic ions [33], with increasing the surface temperature during electron–phonon relaxation, but before reaching the critical temperature for phase explosion initiation.

Such near-surface boiling processes were recently visualized in experiments with a bulk aluminum target slightly below the spallative femtosecond ablation threshold by scanning electron microscopy with high magnification [60]. Traces of homogeneous boiling were observed in the form of nanoscale pits or undersurface cavities at a depth of a few dozen nanometers inside a target [60] (see also [57]). They could easily be visualized using a 15–20 keV electron beam with a penetration depth of initial electrons of about 1–2 μm. Inside a spallative crater for aluminum, copper [125], silver, and gold surfaces [126], intense foaming was observed with the developed residual roughness (Fig. 7). The roughness amplitude increases upon increasing the focusing optics strength due to the increased effect of heat conduction for a smaller focal spot. This roughness represents a self-organized plasmon texture for chemo- and biosensors [126]. These mechanisms of nanoscale relief modification were also used for the ultraprecision ablation of thin films by ultrashort laser pulses [127–134].

Thus, the concepts of the spallative mechanism of femtosecond laser ablation with the frontal detachment of the melt film have been developed over the last two decades from the 'two-wave' model of almost mechanical detachment via the 'single-wave' thermomechanical model to the recent model of the vapor break of the acoustically relaxed (thermally expanded) surface melt. The first and last models represent the extreme mechanisms of the high- and low-temperature liquid–vapor spinodal crossings in the phase diagram (with $T \geqslant T_m$ and $T \leqslant T_{crit}$, where T_m and T_{crit} are the normal melting and critical temperatures of the material). At the same time, even within this approach, where the detachment threshold is related to the undersurface boiling in a thermally expanded melt, a rapid decrease was found in the delay of the detachment onset upon increasing the spallative ablation threshold. This delay tends to characteristic times of the acoustic unloading of the melt and moves into this time range upon reaching the phase explosion threshold and the hydrodynamic critical (nearly critical) or supercritical fluid expansion.

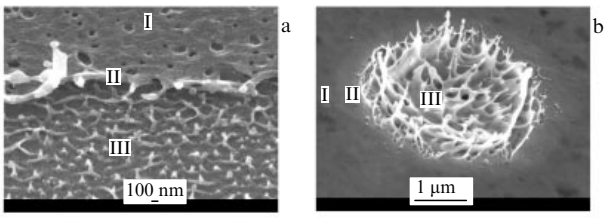

Figure 7. Electron microscope image of the nanoscale roughness of the bottom of spallative craters produced on the surface of (a) bulk aluminum and (b) gold during single-pulse femtosecond laser ablation with the peak fluence above the spallative ablation threshold but below the phase explosion threshold (adapted from [89, 126]). I–III: regions located near, at the edge of, and inside the crater.

4. Hydrodynamic supercritical fluid expansion (phase explosion)

4.1 Brief history and basic research methods

The hydrodynamic lift-off of matter at high internal pressures and temperatures with a strong internal interaction (supercritical fluid, or warm dense matter) during ablation by intense ultrashort laser pulses on the surface of the metals Al, Cu, and W [29] as well as a dielectric and a semimetal (diamond and graphite [28]) was first studied on the picosecond scale by the pump–probe method at high optical pump fluences $\approx 1-10$ J cm^{-2}. It was found that the reflection coefficient decreased by a few times, continuously and monotonically, in fact exponentially, to anomalously low values $\approx 0.1-0.2$, and then gradually returned to the initial level on the subnanosecond time scale. The depth and decay rate of the reflection coefficient depended on the pump fluence. At the same time, a thermodynamic analysis of the ablation process was absent.

A complete thermodynamic analysis of the hydrodynamic lift-off of matter in the ablation phase explosion regime via supercritical states of matter was performed in [40, 41] in comparison with the spallative ablation regime for elucidating the mechanism of the latter. Spallative ablation and the phase explosion were visualized by observing the dynamics of Newton's interference rings in an optical microscope in the time-resolved reflection regime (stationary illumination in the microscope was replaced by a probe ultrashort laser pulse). The phase explosion occurred at higher energy densities at the center of the pump focal spot on the surface, where the interference pattern of Newton's rings was distorted on the subnanosecond scale at picosecond times by the region of a strongly scattering vapor–droplet mixture [31, 59] (see Fig. 5). The structureless exponential decay of the reflection coefficient with the formation of a vapor–droplet mixture was attributed to the adiabatic unloading of a supercritical fluid analyzed using the diagram of states of matter in density–temperature coordinates.

For a similar regime of femtosecond laser ablation of surfaces, the lift-off dynamics of a laser plume were studied by the methods of time-resolved interferometry [30], shadowgraphy [45, 90, 135], time-resolved optical emission spectroscopy [59], probe diagnostics [24], and mass spectrometry [35]. The generation of shock waves in air caused by this lift-off studied by the method of shadowgraphy revealed a distinct correlation between the motion of the plume front and the shock wave front with initial velocities up to a few tens of kilometers per second [46, 90, 135]. Similarly, mass-spectrometric studies in a vacuum revealed the yield of fast ions near the phase explosion threshold with the same velocities to which slow ions from the tail of the ablation plume are added at higher energy densities of ultrashort laser

pulses with a drastic increase in the ablation rate per pulse [35]. More advanced methods for studying the supercritical fluid and plasma, aimed at applications in inertial laser thermonuclear fusion, include X-ray methods with femtosecond time resolution demonstrating the ultrafast disordering of materials (X-ray absorption near-edge spectroscopy) [136], electron dynamics in solids and the plasma–vapor–droplet structure of the laser plume in dynamics (X-ray absorption fine-structure spectroscopy) [43, 137], and superstrong shock waves in matter (X-ray scattering) [138]. However, as a whole, these methods are so far only under development.

4.2 Basic characteristics. The influence of evaporative effects

Experimental and theoretical studies [28, 29, 40, 59, 61, 62, 105, 107, 122, 123] performed earlier have shown that the characteristic time scale of the phase explosion during femtosecond laser ablation is the acoustic unloading time of the critical (supercritical) fluid, equal to the ratio of the surface layer thickness of the fluid to the speed of sound in it. The unloading begins at once after fast, picosecond electron–phonon relaxation. Then, in the case of slow energy transfer from the electron subsystem to the lattice at small electron–phonon coupling constants (for example, for 'good' metals with high electric conductivity, such as gold and silver), it can be expected that the acoustic unloading accompanies the electron–phonon relaxation. But direct comparative investigations for iron [89] with fast electron–phonon relaxation (with the characteristic time of 1–2 ps for the ablation pump level) and the energy deposition rate varied by the ultrashort laser pulse duration showed that the ablation contribution of the phase explosion to crater formation rapidly decreased monotonically with increasing the pulse duration. In particular, the slope of the dependence of the ablation depth on the fluence of an ultrashort laser pulse (the spallative ablation depth being unchanged in this case) monotonically decreases until the complete suppression of this mechanism at durations exceeding 6 ps. These durations are comparable to the acoustic unloading times of a fluid layer (up to 15 ps) removed by the phase explosion for the same fluence of subpicosecond pump laser pulses [89]. Such a suppression of the phase explosion initiated by picosecond laser pulses was attributed to the continuous evaporative cooling of the material surface during electron–phonon relaxation, i.e., even before the achievement of the nearly critical or critical temperature for initiating the phase explosion, which also competes with the continuous hydrodynamic unloading of the produced fluid. The correctness of this explanation seems quite obvious, because picosecond laser pulses are intermediate in their duration between subpicosecond laser pulses (for which spallation and phase explosions are typical ablation mechanisms) and nanosecond (subnanosecond) and longer pulses (with surface evaporation and phase explosions being typical ablation mechanisms). Thus, the beginning of the development of evaporative effects is possible precisely via pumping by picosecond pulses. This is directly confirmed by the results of molecular dynamics calculations [139] showing that surface evaporation considerably affects the type of explosive (bulk) boiling of metals during laser ablation. In addition, it is well known that homogeneous boiling near the critical point is accompanied by a rapid volume increase, thereby acquiring an explosive nature [120] (with the evaporative and hydrodynamic material removing regimes being unified in a certain sense). This leads to a number of new physical phenomena of interest for laser nanotechnologies. For example, the explosive hydrodynamic splashing of a submicron melt from a bath and freezing of a liquid metal jet up to 1 μm in height and up to 100 nm in diameter due to fast lateral nanoscale heat conduction was observed under the double action of an ultrashort laser pulse [140–142].

4.3 Generation of shock waves and mechanical action on a surface

The supercritical character of the initial thermodynamic state of matter (with the energy deposition $\sim 10^5$ J cm^{-3} or more) during the phase explosion upon femtosecond laser ablation at high pump fluence $\approx 1-10$ J cm^{-2} causes the fast hydrodynamic expansion of the material [30, 43, 46, 59, 90, 135–138]. The fast energy release followed by electron–phonon relaxation (energy depositions $\sim 10^5$ J cm^{-3}) or plasma formation (energy depositions $\sim 10^6$ J cm^{-3} or higher) should lead to the 'table-top' generation of superpower pressure waves (at the megabar level $\sim 10^2-10^3$ GPa) along with the ablation of material in the absorbing surface layer of the target [45, 46, 55, 104, 124, 143–145]. This is terminated by the generation of high-power shock waves in the target. Because the detection of pressure waves on the rear side of the target by standard interferometric optical methods such as VISAR (velocity interferometer system for any reflector), ORVIS (optical recording VISAR), and femtosecond interference microscopy [57, 101–103, 124, 146] cannot give the pressure value in the ablation source due to the strong dissipation of a shock wave already at the micrometer scale [143, 146], while the use of submicron foils or films (on substrates) is not always possible (especially in technological applications [145]), it is interesting to perform such studies on the front side of the target by estimating the initial pressure in the source in terms of the expansion parameters of a laser plume. However, in the regime of generation of subcritical erosion plasma (with the ultrashort pulse intensity below 10^{14} W cm^{-2} [30]), the opacity of the laser plume and scattering of light from it prevent frontal interferometric [30, 45, 56] or reflectometric measurements [31, 59, 122] of its expansion velocity. At the same time, during the expansion of a dense laser plume in air, high-power shock waves appear, which are transformed into sonic waves in the far acoustic zone and can be detected with broadband ultrasonic piezoelectric sensors [55, 143–145] for different materials (metals and graphite), depending on the fluence of the ultrashort laser pulse. One of the advantages of this method for studying shock waves in air during the expansion of the supercritical fluid plume is the possibility of frontal measurements of the mean velocity of a shock wave in air for any geometry of the experiment and any target surface profile, in contrast to other methods of dynamic optical diagnostics with lateral visualization (spatial resolution) in the near acoustic zone, such as shadowgraphy [45, 90, 135], optical emission photography, or spectroscopy [59]. As a result, in fact the only systematic results on ablation pressures, velocities, and characteristic expansion times of the laser plume were obtained by this ultrasonic method [55, 143–145], which was also used for comparing ablation pressures on the front side and pressures of the compression wave on the rear side of the target.

In particular, ultrasonic studies have been used to measure microsecond propagation times, the submicrosecond half-width, and the amplitude of pressure wave pulses as functions of the fluence and focal spot radius of an

ultrashort laser pulse and the wave propagation distance from the ablation zone to an ultrasonic sensor [55, 143–145]. The measurements were performed by the leading edge of a bipolar pressure pulse differentiated due to diffraction [147] (a monopolar compression pulse in the source). In this case, the transit time monotonically decreased above the phase explosion threshold on the target surface irradiated by an ultrashort laser pulse, while the pulse half-width and amplitude increased. Experimental data were processed using a program algorithm with the dependences of the transit time and half-width of the pressure wave pulse on the fluence and the laser focal spot radius taken into account. Also, transit distances from the ablation zone to a highly sensitive ultrasonic sensor were taken into account for two stages: the supersonic and sonic motion, where the sound speed was taken for normal conditions. The first stage is realized during the expansion of the ablation piston plume accelerating a shock wave in air, which was simulated by the point explosion of a region of material with the initial radius equal to the ablation zone radius on the target surface for the given fluence of the laser pulse, varied by the initial pressure of the plume. The initial and instant expansion rates of the plume and shock wave are determined by the initial and instant pressures on the plume front via classical relations in the point explosion theory [148]. This stage proceeds until the pressure reaches the transient value (about 6 atm in air). At the second stage, the pressure wave propagates in the sonic regime. The total transit time at both stages calculated as a function of the initial pressure for the ablation region size fixed for a given radiation fluence is compared with the experimental transit time, and the initial pressure is determined from the best fit.

This method allows finding the initial pressure and expansion rate of the ablation plume in air for different materials as functions of the parameters mentioned above and relating them to parameters of output pressure waves on the rear side of the target. The method was used to study the propagation and interaction of superpower ($\sim 10^2-10^3$ GPa) shock waves with materials [149, 150] or with the improved strength (hardness and resistance to cracks) and corrosive characteristics of the surface layer of materials strengthened by laser-induced shock waves [151–153]. This method can also be used for contact-free quantitative diagnostics of these phenomena in the condensed phase and to control the regimes of its processing by ultrashort laser pulses. We note that it was erroneously assumed in [154] that shock-wave loading of the surface layer of materials during their ablation by ultrashort laser pulses proceeds at a picosecond time scale; it was shown in [144, 145] by using ultrasonic diagnostics and numerical calculations that in reality the loading of the surface after the action of an ultrashort laser pulse continues at the submicrosecond time scale of the ablation plume expansion. These results are quantitatively confirmed by the data of spatially and time-resolved optical emission spectroscopy of single-pulse ablation plumes presenting their velocities and characteristic expansion times measured depending on the fluence of ultrashort pump laser pulses [59].

Acoustic measurements performed for high-power shock waves [144] (with pressures $\sim 10^2-10^3$ GPa) on the front and rear sides of the ablated target confirmed their superelastic propagation, which was earlier observed for lower-power shock waves (pressures $\sim 10-10^2$ GPa) and was theoretically predicted in [150]. In this case, for weaker shock waves (with pressures $\sim 1-10$ GPa), the superelastic propagation changes to more dissipative propagation, with the generation of residual stresses at the GPa level [144, 145] attributed in [146, 155] to assumed shock-wave structural transformations in iron and vanadium. Unlike frontal ablation, shock waves were excited in a metal film in [146, 155] by focusing ultrashort laser pulses through a glass substrate of the film, which allowed studying the strength of various materials with respect to tensile stresses for very high deformation rates ($\sim 10^9$ s^{-1}) in solids [146, 149, 155] rather than melts [124].

It is of interest that ablation pressures $\sim 10-10^3$ GPa measured in the phase explosion regime by ultrasonic and optical emission and interferometric methods [30, 45, 46, 55, 59, 84, 124, 135, 143, 144, 156, 157] considerably exceed pressures ~ 10 GPa calculated recently by the hybrid two-temperature model–molecular dynamics method [61, 62]. Although the so-called electron pressure was recently introduced [83–87] to such models to describe ablation by ultrashort pulses (USPs), it seems that the discrepancy between experiments and the theory is mainly related to the mechanism of ultrafast laser plasma ablation [51–53, 80, 81] considered in Section 1. Both the subpicosecond plasma yield itself [28] and plasma heating by a pump USP [24] can increase the pressure to a value considerably exceeding the critical pressure of a material. This assumption is confirmed by good agreement between achieved pressures $\sim 10-10^3$ GPa and the pressures $P_{\rm cr} \sim 1$ TPa in an isothermic critical plasma with the atomic mass M and the average ion charge $\langle Z \rangle$ under comparable conditions of irradiation by ultrashort pulses ($I_{\rm las} \sim 1 \times 10^2$ TW cm^{-2}), for example, calculated from the relation [45]

$$P_{\rm cr} = 2\rho_{\rm cr} C_{\rm plas}^2 = 12\left(\frac{I}{10^2\ \text{TW cm}^{-2}}\right)^{2/3}\left(\frac{1\ \mu\text{m}}{\lambda_{\rm las}}\right)^{2/3} \times \left(\frac{M}{2\langle Z\rangle}\right)^{1/3} [\text{Mbar}]\,, \qquad I = 4\rho_{\rm cr} C_{\rm plas}^3\,, \tag{5}$$

where the wavelength is $\lambda_{\rm las} \sim 1$ μm and the expansion rate at the critical plasma boundary $C_{\rm plas} \sim 1 \times 10^2$ km s^{-1} is determined by the second (balance) equation in (5). In fact, the ultrafast plasma yield and its simultaneous heating by ultrashort laser pulses already in the gas phase embody the expected but not yet experimentally observed gradual transition from a strongly heated electron gas in a solid to a low-temperature erosion plasma with a monotonic increase in pressure with increasing the ultrashort laser pulse fluence according to the corresponding increase in the volume density of the deposited energy [136, 137].

5. Conclusions

The analysis of work considered above shows that the predetermined dynamics of a long multiscale chain of different electronic and lattice processes during femtosecond laser ablation, which is not directly affected by the initiating ultrashort laser pulse, allows the elucidation in principle of fundamental ablation mechanisms. This review shows that such studies can be performed in stages, beginning with the absorption of an ultrashort laser pulse to the ablation of a material and ending with thermal relaxation. The review outlines the main mechanisms of femtosecond laser ablation and presents their phenomenological picture, implying further theoretical simulations for constructing the complete

picture and universal detailed description of this complex but very interesting and important physical phenomenon. At the same time, the various mechanisms of femtosecond laser ablation considered above give rise to a variety of applications of laser ablation in processing material surfaces and nanotechnologies, which undoubtedly deserves a separate large review.

Acknowledgments
The work of A A I was supported by the Russian Science Foundation (project No. 15-19-00208). The work of S I K was supported by the Government of the Russian Federation (grant no. 074-U01) via the ITMO Visiting Professorship Program.

References

1. Prokhorov A M, Anisimov S I, Pashinin P P *Sov. Phys. Usp.* **19** 547 (1976); *Usp. Fiz. Nauk* **119** 401 (1976)
2. Afanas'ev Yu V, Isakov V A, Krokhin O N *Sov. Phys. JETP* **54** 910 (1981); *Zh. Eksp. Teor. Fiz.* **81** 1714 (1981)
3. Agranat M B et al. *JETP Lett.* **30** 167 (1979); *Pis'ma Zh. Eksp. Teor. Fiz.* **30** 182 (1979)
4. Liu J M et al. *Appl. Phys. Lett.* **39** 755 (1981)
5. Yen R et al. *Appl. Phys. A* **27** 153 (1982)
6. Kryukov P G *Femtosekundnye Impul'sy. Vvedenie v Novuyu Oblast' Lazernoi Fiziki* (Femtosecond Pulses. Introduction to a New Field of Laser Physics) (Moscow: Fizmatlit, 2008); *Phys. Usp.* **56** 849 (2013); *Usp. Fiz. Nauk* **183** 897 (2013); *Phys. Usp.* **58** 762 (2015); *Usp. Fiz. Nauk* **185** 817 (2015)
7. Anisimov S I, Kapeliovich B L, Perel'man T L *Sov. Phys. JETP* **39** 375 (1974); *Zh. Eksp. Teor. Fiz.* **66** 776 (1974)
8. Allen P B *Phys. Rev. Lett.* **59** 1460 (1987)
9. Akhmanov S A et al. *Sov. Phys. Usp.* **28** 1084 (1985); *Usp. Fiz. Nauk* **147** 675 (1985)
10. Bäuerle D *Laser Processing and Chemistry* (Berlin: Springer, 2000)
11. Koroteev N I, Shumai I L *Fizika Moshchnogo Lazernogo Izlucheniya* (Physics of High-Power Laser Radiation) (Moscow: Nauka, 1991)
12. Veiko V P et al. *Vzaimodeistvie Lazernogo Izlucheniya s Veshchestvom: Silovaya Optika* (Interaction of Laser Radiation with Matter: High-Power Optics) (Moscow: Fizmatlit, 2008)
13. Anisimov S I, Luk'yanchuk B S *Phys. Usp.* **45** 293 (2002); *Usp. Fiz. Nauk* **172** 301 (2002)
14. Wellershoff S S et al. *Appl. Phys. A* **69** S99 (1999)
15. Agranat M B et al. *JETP Lett.* **101** 598 (2015); *Pis'ma Zh. Eksp. Teor. Fiz.* **101** 671 (2015)
16. Glezer E N et al. *Phys. Rev. B* **51** 6959 (1995)
17. Kudryashov S I et al. *Phys. Rev. B* **75** 085207 (2007)
18. Apostolova T et al. *Opt. Eng.* **51** 121808 (2012)
19. Reitze D H et al. *Phys. Rev. B* **40** 11986(R) (1989)
20. Golosov E V et al. *JETP* **113** 14 (2011); *Zh. Eksp Teor. Fiz.* **140** 21 (2014)
21. Wang X Y et al. *Phys. Rev. B* **50** 8016 (1994)
22. Fujimoto J G et al. *Phys. Rev. Lett.* **53** 1837 (1984)
23. Ang L K, Pant M *Phys. Plasmas* **20** 056705 (2013)
24. Amoruso S et al. *Appl. Surf. Sci.* **186** 358 (2002)
25. Anisimov S I, Benderskii V A, Farkas G *Phys. Usp.* **20** 467 (1977); *Usp. Fiz. Nauk* **122** 185 (1977)
26. Shank C V, Yen R, Hirlimann C *Phys. Rev. Lett.* **50** 454 (1983)
27. Downer M C, Fork R L, Shank C V *J. Opt. Soc. Am. B* **2** 595 (1985)
28. Reitze D H, Ahn H, Downer M C *Phys. Rev. B* **45** 2677 (1992)
29. Wang X Y, Downer M C *Opt. Lett.* **17** 1450 (1992)
30. Evans R et al. *Phys. Rev. Lett.* **77** 3359 (1996)
31. Von der Linde D, Sokolowski-Tinten K *Appl. Surf. Sci.* **154–155** 1 (2000)
32. Von der Linde D, Sokolowski-Tinten K, Bialkowski J *Appl. Surf. Sci.* **109–110** 1 (1997)
33. Cavalleri A et al. *J. Appl. Phys.* **85** 3301 (1999)
34. Schmidt V, Husinsky W, Betz G *Phys. Rev. Lett.* **85** 3516 (2000)
35. Ye M, Grigoropoulos C P *J. Appl. Phys.* **89** 5183 (2001)
36. Hulin D et al. *Phys. Rev. Lett.* **52** 1998 (1984)
37. Preuss S, Demchuk A, Stuke M *Appl. Phys. A* **61** 33 (1995)
38. Chichkov B N et al. *Appl. Phys. A* **63** 109 (1996)
39. Sokolowski-Tinten K et al. *Proc. SPIE* **3343** 46 (1998)
40. Sokolowski-Tinten K et al. *Phys. Rev. Lett.* **81** 224 (1998)
41. Anisimov S I et al. *JETP Lett.* **77** 606 (2003); *Pis'ma Zh. Eksp. Teor. Fiz.* **77** 731 (2003)
42. Perez D, Lewis L J *Phys. Rev. Lett.* **89** 255504 (2002)
43. Oguri K et al. *Phys. Rev. Lett.* **99** 165003 (2007)
44. Norman G E et al. *Contrib. Plasma Phys.* **53** 129 (2013)
45. Batani D et al. *Phys. Rev. E* **68** 067403 (2003)
46. Zeng X et al. *Appl. Phys. A* **80** 237 (2005)
47. Vailionis A et al. *Nature Commun.* **2** 445 (2011)
48. Korte F et al. *Appl. Phys. A* **77** 229 (2003)
49. Joglekar A P et al. *Proc. Natl. Acad. Sci. USA* **101** 5856 (2004)
50. Shinoda M, Gattass R R, Mazur E *J. Appl. Phys.* **105** 053102 (2009)
51. Ionin A A et al. *Appl. Phys. A* **117** 1757 (2014)
52. Ionin A A et al. *JETP Lett.* **101** 308 (2015); *Pis'ma Zh. Eksp. Teor. Fiz.* **101** 336 (2015)
53. Ionin A A et al. *Laser Phys. Lett.* **12** 075301 (2015)
54. Danilov P A et al. *JETP* **120** 946 (2015); *Zh. Eksp. Teor. Fiz.* **147** 1098 (2015)
55. Zhakhovskii V V, Inogamov N A, Nishihara K *JETP Lett.* **87** 423 (2008); *Pis'ma Zh. Eksp. Teor. Fiz.* **87** 491 (2008)
56. Ionin A A et al. *JETP Lett.* **94** 266 (2011); *Pis'ma Zh. Eksp. Teor. Fiz.* **94** 289 (2011)
57. Ashitkov S I et al. *JETP Lett.* **95** 176 (2012); *Pis'ma Zh. Eksp. Teor. Fiz.* **95** 192 (2012)
58. Ionin A A et al. *JETP Lett.* **96** 375 (2012); *Pis'ma Zh. Eksp. Teor. Fiz.* **96** 413 (2012)
59. Ionin A a et al. *JETP* **116** 347 (2013); *Zh. Eksp. Teor. Fiz.* **143** 403 (2013)
60. Ionin A A et al. *Laser Phys. Lett.* **13** 025603 (2015)
61. Wu C, Zhigilei L V *Appl. Phys. A* **114** 11 (2014)
62. Ivanov D S et al. *Appl. Phys. A* **117** 2133 (2014
63. Isakov V A, Kanavin A P, Uryupin S A *Quantum Electron.* **36** 928 (2006); *Kvantovaya Elektron.* **36** 928 (2006)
64. Lin Z, Zhigilei L V, Celli V *Phys. Rev. B* **77** 075133 (2008)
65. Petrov Yu V, Inogamov N A, Migdal K P *JETP Lett.* **97** 20 (2013); *Pis'ma Zh. Eksp. Teor. Fiz.* **97** 24 (2013)
66. Tom H W K, Aumiller G D, Brito-Cruz C H *Phys. Rev. Lett.* **60** 1438 (1988)
67. Saeta P et al. *Phys. Rev. Lett.* **67** 1023 (1991)
68. Sokolowski-Tinten K et al. *Appl. Phys. A* **53** 227 (1991)
69. Sokolowski-Tinten K et al. *Nature* **422** 287 (2003)
70. Bulgakova N M et al. *Phys. Rev. B* **69** 054102 (2004)
71. Rethfeld B et al. *Appl. Phys. A* **101** 19 (2010)
72. Shcheblanov N S, Itina T E *Appl. Phys. A* **110** 579 (2013)
73. Lenner M et al. *Phys. Rev. B* **79** 184105 (2009)
74. Dachraoui H, Husinsky W *Phys. Rev. Lett.* **97** 107601 (2006)
75. Huang M et al. *Phys. Rev. B* **79** 125436 (2009)
76. Hebeisen C T et al. *Phys. Rev. B* **78** 081403(R) (2008)
77. Zhao X, Shin Y C *J. Phys. D* **46** 335501 (2013)
78. Roeterdink W G et al. *Appl. Phys. Lett.* **82** 4190 (2003)
79. Stoian R et al. *Appl. Phys. Lett.* **85** 694 (2004)
80. Ionin A A et al. *Bull. Russ. Acad. Sci. Phys.* **80** 450 (2016); *Izv. Ross. Akad. Nauk Ser. Fiz.* **80** 495 (2016)
81. Hada M et al. *Nature Commun.* **5** 3863 (2014)
82. Kudryashov S I, Emel'yanov V I *JETP Lett.* **73** 666 (2001); *Pis'ma Zh. Eksp. Teor. Fiz.* **73** 751 (2001)
83. Gamaly E et al. *Phys. Plasmas* **9** 949 (2002)
84. Itina T E et al. *Thin Solid Films* **453–454** 513 (2004)
85. Inogamov N A et al. *Contrib. Plasma Phys.* **53** 796 (2013)
86. Stegailov V, Zhilyaev P *Contrib. Plasma Phys.* **55** 164 (2015)
87. Starikov S V, Pisarev V V *J. Appl. Phys.* **117** 135901 (2015)
88. Ashcroft N W, Mermin N D *Solid State Physics* (New York: Holt, Rinehart and Winston, 1976); Translated into Russian: *Fizika Tverdogo Tela* (Moscow: Mir, 1979)
89. Artyukov I A et al. *JETP Lett.* **99** 51 (2014); *Pis'ma Zh. Eksp. Teor. Fiz.* **99** 54 (2014)
90. Choi T Y, Grigoropoulos C P *J. Appl. Phys.* **92** 4918 (2002)
91. Bogatyrev I B et al. *J. Appl. Phys.* **110** 103106 (2011)

92. Girardeau-Montaut J P, Girardeau-Montaut C *Phys. Rev. B* **51** 13560 (1995)
93. Zayarny D A et al. *JETP Lett.* **103** 752 (2016); *Pis'ma Zh. Eksp. Teor. Fiz.* **103** 752 (2016)
94. Zayarny D A et al. *Laser Phys. Lett.* **13** 076101 (2016)
95. Bashir S, Rafique M S, Husinsky W *Nucl. Instrum. Meth. Phys. Res. B* **275** 1 (2012)
96. Ionin A A et al. *Laser Phys. Lett.* **10** 056004 (2013)
97. Nathala C S R et al. *Opt. Exp.* **23** 5915 (2015)
98. Kudryashov S I et al. *Opt. Lett.* **40** 4967 (2015)
99. Ionin A A et al. *JETP Lett.* **101** 350 (2015); *Pis'ma Zh. Eksp. Teor. Fiz.* **101** 382 (2015)
100. Anisimov S I, Prokhorov A M, Fortov V E *Sov. Phys. Usp.* **27** 181 (1984); *Usp. Fiz. Nauk* **142** 395 (1984)
101. Kanel G I et al. *Udarno-volnovye Yavleniya v Kondensirovannykh Sredakh* (Ssock-Wave Phenomena in Condensed Media) (Moscow: Yanus-K, 1996)
102. Krasyuk I K et al. *Quantum Electron.* **33** 593 (2003); *Kvantovaya Elektron.* **33** 593 (2003)
103. Kanel G I, Fortov V E, Razorenov S V *Phys. Usp.* **50** 771 (2007); *Usp. Fiz. Nauk* **177** 809 (2007)
104. Ionin A A et al. *JETP* **148** 846 (2015); *Pis'ma Zh. Eksp. Teor. Fiz.* **148** 846 (2015)
105. Leveugle E, Ivanov D S, Zhigilei L V *Appl. Phys. A* **79** 1643 (2004)
106. Zhigilei L V, Lin Z, Ivanov D S *J. Phys. Chem. C* **113** 11892 (2009)
107. Demaske B J et al. *Phys. Rev. B* **82** 064113 (2010)
108. Lorazo P, Lewis L J, Meunier M *Phys. Rev. B* **73** 134108 (2006)
109. Sonntag S et al. *Appl. Phys. A* **104** 559 (2011)
110. Paltauf G, Schmidt-Kloiber H *Appl. Phys. A* **62** 303 (1996)
111. Kim D, Ye M, Grigoropoulos C P *Appl. Phys. A* **67** 169 (1998)
112. Kudryashov S I et al. *J. Appl. Phys.* **100** 056103 (2006)
113. Kudryashov S I, Allen S D *Appl. Phys. A* **79** 1737 (2004)
114. Lang F et al. *Appl. Phys. Lett.* **85** 2759 (2004)
115. Kudryashov S I, Allen S D *J. Appl. Phys.* **95** 5820 (2004)
116. Kudryashov S I, Allen S D *J. Appl. Phys.* **93** 4306 (2003)
117. Kudryashov S I, Allen S D *J. Appl. Phys.* **100** 104908 (2006)
118. Kudryashov S I, Lyon K, Allen S D *Phys. Rev. E* **73** 055301(R) (2006)
119. Kudryashov S I, Lyon K, Allen S D *Phys. Rev. E* **75** 036313 (2007)
120. Skripov V P et al. *Thermophysical Properties of Liquids in the Metastable* (*Superheated*) *State* (New York: Gordon and Breach Sci. Publ., 1988); Translated from Russian: *Teplofizicheskie Svoistva Zhidkostei v Metastabil'nom Sostoyanii* (Moscow: Atomizdat, 1980)
121. Ionin A A et al. *Appl. Phys. B* **111** 419 (2013)
122. Ionin A A et al. *JETP Lett.* **94** 753 (2011); *Pis'ma Zh. Eksp. Teor. Fiz.* **94** 816 (2011)
123. Kudryashov S I, Ionin A A *Int. J. Heat Mass Transfer* **99** 383 (2016)
124. Ashitkov S I et al. *JETP Lett.* **103** 544 (2016); *Pis'ma Zh. Eksp. Teor. Fiz.* **103** 611 (2016)
125. Oboňa J V et al. *Appl. Surf. Sci.* **303** 118 (2014)
126. Kuchmizhak A et al. *ACS Appl. Mater. Interfaces* **8** 24946 (2016)
127. Korte F et al. *Appl. Phys. A* **77** 229 (2003)
128. Koch J et al. *Appl. Phys. A* **81** 325 (2005)
129. Nakata Y, Miyanaga N, Okada T *Appl. Surf. Sci.* **253** 6555 (2007)
130. Reininghaus M et al. *Opt. Exp.* **31** 32176 (2013)
131. Danilov P A et al. *Quantum Electron.* **44** 540 (2014); *Kvantovaya Elektron.* **44** 540 (2014)
132. Danilov P A et al. *Appl. Phys. A* **117** 981 (2014)
133. Kuchmizhak A et al. *Sci. Rep.* **6** 19410 (2016)
134. Kuchmizhak A et al. *Nanoscale* **8** 12352 (2016)
135. Zhang N et al. *Phys. Rev. Lett.* **99** 167602 (2007)
136. Leguay P M et al. *Phys. Rev. Lett.* **111** 245004 (2013)
137. Cho B I et al. *Phys. Rev. Lett.* **106** 167601 (2011)
138. Fletcher L B et al. *Nature Photon.* **9** 274 (2015)
139. Mazhukin V I et al. *Quantum Electron.* **44** 283 (2014); *Kvantovaya Elektron.* **44** 283 (2014)
140. Gubko M A et al. *JETP Lett.* **97** 599 (2013); *Pis'ma Zh. Eksp. Teor. Fiz.* **97** 687 (2013)
141. Gubko M A et al. *Laser Phys. Lett.* **11** 065301 (2014)
142. Ionin A A et al. *Bull. Russ. Acad. Sci. Phys.* **80** 991 (2016); *Izv. Ross. Akad. Nauk Ser. Fiz.* **80** 1080 (2016)
143. Kudryashov S I et al. *AIP Conf. Proc.* **1464** 244 (2012)
144. Ageev E I et al. *JETP Lett.* **102** 693 (2015); *Pis'ma Zh. Eksp. Teor. Fiz.* **102** 785 (2015)
145. Ageev E I et al. *Appl. Phys. Lett.* **108** 084106 (2016)
146. Ashitkov S I et al. *JETP Lett.* **101** 276 (2015); *Pis'ma Zh. Eksp. Teor. Fiz.* **101** 294 (2015)
147. Gusev V E, Karabutov A A *Laser Optoacoustics* (New York: AIP, 1993)
148. Zel'dovich Ya B, Raizer Yu P *Physics of Shock Waves and High-Temperature Hydrodynamic Phenomena* (Mineola, NY: Dover Publ., 2002); Translated from Russian: *Fizika Udarnykh Voln i Vysokotemperaturnykh Gazodinamicheskikh Yavlenii* (Moscow: Nauka, 1966)
149. Ashitkov S I et al. *JETP Lett.* **92** 516 (2010); *Pis'ma Zh. Eksp. Teor. Fiz.* **92** 568 (2010)
150. Inogamov N A et al. *JETP Lett.* **93** 226 (2011); *Pis'ma Zh. Eksp. Teor. Fiz.* **93** 245 (2011)
151. Lee D, Kannatey-Asibu E (Jr.) *J. Laser Appl.* **23** 022004 (2011)
152. Ye Y, Feng Y, Lian Z, Hua Y *Appl. Surf. Sci.* **309** 240 (2014)
153. Ye Y, Feng Y, Lian Z, Hua Y *Opt. Laser Eng.* **67** 74 (2015)
154. Wu B, Tao S, Lei S *Appl. Surf. Sci.* **256** 4376 (2010)
155. Ashitkov S I et al. *JETP Lett.* **98** 384 (2013); *Pis'ma Zh. Eksp. Teor. Fiz.* **98** 439 (2013)
156. Sano T et al. *Appl. Surf. Sci.* **247** 571 (2005)
157. Yang J et al. *Phys. Rev. B* **76** 165430 (2007)